


Moiré pattern of a spin liquid and a Néel magnet in the Kitaev modelR. Wang , P. Wang, K. L. Zhang , and Z. Song ^{*}
School of Physics, Nankai University, Tianjin 300071, China (Received 29 October 2019; revised 4 September 2020; accepted 5 September 2020; published 30 September 2020)

A moiré pattern occurs when two periodic structures in a system have a slightly mismatched period, resulting in the coexistence of distinct phases in different large-scale spatial regions of the same system. The periodic structures can arise from the intrinsic crystalline order or periodic external field. We investigate the moiré pattern using a dimerized Kitaev spin model with a periodic transverse field, which can be mapped onto the system of dimerized spinless fermions with p -wave superconductivity or a quasi-one-dimensional Su-Schrieffer-Heeger Majorana lattice. The exact solution for the staggered field demonstrated that the ground state has two distinct phases: a Néel magnetic phase for the nonzero field and a spin liquid phase due to the emergence of an isolated flat Bogoliubov–de Gennes band for the vanishing field. We compute the staggered magnetization and local density of state for the field with a slightly different period of the lattice. The numerical simulation demonstrates that two such phases appear alternatively along the system with a long beat period. Additionally, we propose a dynamic scheme, via a evanescently coupled-waveguide array, to detect the moiré fringes based on the measurement of the Loschmidt echo in the presence of local perturbations.

DOI: [10.1103/PhysRevB.102.094207](https://doi.org/10.1103/PhysRevB.102.094207)**I. INTRODUCTION**

Moiré patterns emerge due to the superposition of two periodic structures, with either slightly different periods or different orientations; such patterns have been realized in materials [1–7]. Recently, the influence of moiré patterns in physical systems has attracted considerable interest. Moiré patterns have been extensively studied [2–4, 8–11] as a new technique to apply periodic potentials in van der Waals heterostructures to tune their electronic properties. Many notable phenomena have been observed in heterostructure materials with small twist angles and mismatched lattice constants. Moiré patterns in condensed-matter systems are produced by the difference in lattice constants or the orientation of two two-dimensional lattices when they are stacked into a two-layer structure.

Most studies have focused on quasi-two-dimensional systems; one-dimensional moiré systems have been much less investigated and are expected to be easily realized in an artificial system. Generally, moiré patterns are the result of competition between at least two effects on electrons that are critical for both applications and fundamental physics. These patterns can be the periodic appearance of two different quantum phases, exhibiting unprecedented states of matter. In principle, a one-dimensional moiré system can be deliberately designed (engineered) as a superlong-period system when the periods of two ingredients are slightly different but commensurate. It is essentially a periodic system with a huge unit cell, which is large enough to exhibit the signatures of various quantum phases. It also displays the crossover or quantum phase transition as the coordinate changes in real

space, rather than varying the external field. It is interesting to study the quantum phase transition in such a moiré system, which provides another way to demonstrate the phase diagram. An advantage of this scheme is that one does not need to control the field dynamically.

Theoretically, two periodic structures can arise from the intrinsic crystalline order or periodic external field. In condensed matter, particles are usually confined by a periodic potential in synthetic and natural materials. Another periodic structure can come from an external field, such as a periodic magnetic field, which takes effects on the spin degree of freedom of the particles. Alternatively, it can also come from another periodic potential, which takes effects on the tunneling amplitudes. In Fig. 1 we schematically illustrate such a scheme by a sample of coupled resonator array [12, 13], which can be employed to mimic a quasi-one-dimensional Su-Schrieffer-Heeger (SSH) model with moiré structure. One relevant example is the Kitaev spin model [Eq. (1)], which demonstrates the two mechanisms. On the one hand, it describes electrons in a periodic potential or an ultracold atom in a Mott-insulating phase, while the magnetic field has a slightly mismatched period. On the other hand, a Kitaev model has a Majorana representation, which is a quasi-one-dimensional SSH lattice [14, 15].

In this paper we investigate the moiré pattern that emerges in a dimerized Kitaev spin model with a periodic transverse field. The exact solution for the staggered field demonstrates two distinct phases for the ground states. The strong field results in a Néel ordered spin array, whereas the spin-liquid phase emerges for the zero field due to the isolated flat Bogoliubov–de Gennes band. When the period of the transverse field results in a slightly mismatched lattice constant, the local properties, such as local staggered magnetization and local density of state (LDOS), vary periodically along the

^{*}songtc@nankai.edu.cn

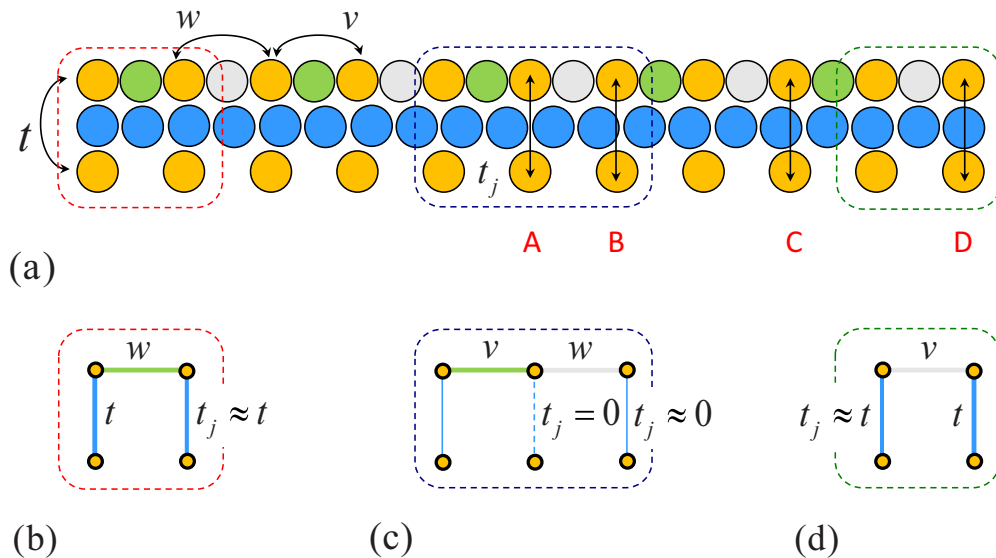


FIG. 1. Schematic illustration of a one-dimensional moiré system, which consists two ingredients with slightly different but commensurate periods. (a) Schematic of the coupled resonator array. The auxiliary resonators (green, gray, and blue dots) induce the effective couplings between primary resonators (yellow dots). The ratio between the diameters of upper and middle circles is 20/21, obtained by the numbers of two kinds of circles. The mismatch between primary and auxiliary resonators results in nonuniform coupling strength t_j between upper and lower primary resonators. For instance, it is reasonable to use the segment length of the vertical double-arrow line in the blue dot to measure the value of t_j . At the middle A, a vertical double-arrow line has vanishing segment length, resulting in $t_j = 0$ [dotted line in (c)], while we get the maximal value of $t_j = t$ [thick lines in (b) and (d)] at the end of D. Accordingly, we have $t_j \approx 0$ [thin lines in (c)] at B, and $t_j \approx t$ at C. For a long system, the distribution of $\{t_j\}$ leads to a long-period structure. Other two auxiliary resonators (green and gray dots) induce staggered couplings (w and v) along the ladder. (b)–(d) Schematic representative lattice structures of the moiré system in (a).

system with a long beat period, indicating that Néel and spin-liquid phases appear alternatively. We also propose a dynamic scheme to detect the moiré fringes experimentally. The underlying mechanism is based on the relationship between the decay rate of Loschmidt echo (LE) and the LDOS when a local perturbation is added. Numerical simulation demonstrates that the decay rate exhibits the same periodic behavior as the other quantities. It provides a method for detecting the moiré fringes in a photonic SSH model via LE in a coupled waveguide array, where time-reversal evolution is simulated by the aid of segmented sections [16,17].

This paper is organized as follows. In Sec. II we present a dimerized Kitaev spin model with spatially modulated transverse fields. In Sec. III we introduce the concepts of magnetization, density of state (DOS), and string correlation function to characterize related ground-state properties. In Sec. IV we discuss moiré fringes in the model. In Sec. V we propose a dynamic scheme to experimentally detect the moiré fringes. Finally, we provide a summary in Sec. VI.

II. MODEL HAMILTONIAN

We commenced our investigation by considering a dimerized Kitaev spin with spatially modulated transverse fields

$$H = \sum_{j=1}^N [(1 - \delta)\sigma_{2j-1}^x \sigma_{2j}^x + (1 + \delta)\sigma_{2j}^y \sigma_{2j+1}^y] + \sum_{j=1}^{2N} g_j \sigma_j^z, \quad (1)$$

where σ_j^α ($\alpha = x, y, z$) are the Pauli operators on site j and $g_j = g \cos[\pi(1 + \Delta)j]$. We take $\sigma_{2N+1}^y \equiv \sigma_1^y$ to impose a periodic boundary condition. The main results of this work are independent of the boundary conditions. The case of the zero-field ($g = 0$) has been studied in many perspectives [18–20]. In the case of the staggered-field ($\Delta = 0$), that is, the transverse field parameter in Eq. (1) satisfy $g_{2j-1} = -g_{2j}$, where $j = 1, 2, \dots, N$, previous work [21] has focused on the topological feature of the degeneracy lines. For an arbitrary parameter distribution function g_j , we have an equivalent dimerized spinless fermion model with the Hamiltonian

$$H = \sum_{j=1}^N [(1 - \delta)(c_{2j-1}^\dagger c_{2j}^\dagger + c_{2j-1}^\dagger c_{2j}) + (1 + \delta)(c_{2j+1}^\dagger c_{2j}^\dagger + c_{2j}^\dagger c_{2j+1}) + \text{H.c.}] + \sum_{j=1}^{2N} g_j (1 - 2c_j^\dagger c_j), \quad (2)$$

which describes p -wave superconductivity. Here c_j is a spinless fermionic operator, and this mapping is obtained with the Jordan-Wigner transformation [22]

$$\begin{aligned} \sigma_j^x &= - \prod_{l < j} (1 - 2c_l^\dagger c_l) (c_j^\dagger + c_j), \\ \sigma_j^y &= -i \prod_{l < j} (1 - 2c_l^\dagger c_l) (c_j^\dagger - c_j), \\ \sigma_j^z &= 1 - 2c_j^\dagger c_j. \end{aligned} \quad (3)$$

The on-site external field is extracted from the continuous field $g(x) = g \cos[\pi(1 + \Delta)x]$ in the continuous coordinate x , with the period $2/(1 + \Delta)$. For a sufficiently small Δ , we have $g_j \approx g_{\text{eff}} \cos(\pi j)$, where $g_{\text{eff}} = g \cos(\pi \Delta j)$ varies slowly. To a small extent, g_j can be regarded as a staggered magnetic field with amplitude $|g_{\text{eff}}|$. For a long scale, $|g_{\text{eff}}|$ is a periodic function of j with the beat period $2/\Delta$, that is, the amplitude of the magnetic field is a constant in the narrow interval but varies periodically along the whole system. To investigate the local properties of the system within a small region, we consider the Hamiltonian as a homogeneous one, that is, with zero Δ but varied g . The ground-state properties with different g reflect the local properties of the original Hamiltonian within different space regions.

We impose the periodic boundary condition $\sigma_j^\alpha \equiv \sigma_{j+2N}^\alpha$ and perform the Fourier transformations for the two sublattices, which obey

$$c_j = \frac{1}{\sqrt{N}} \sum_k e^{ikl} \begin{cases} \alpha_k, & j = 2l - 1, \\ \beta_k, & j = 2l, \end{cases} \quad (4)$$

where $l = 1, 2, \dots, N$, $k = 2m\pi/N$, $m = 0, 1, 2, \dots, N - 1$. Thus, spinless fermionic operators in k space, α_k, β_k can be expressed as

$$\begin{aligned} \alpha_k &= \frac{1}{\sqrt{N}} \sum_l e^{-ikl} c_j, & j = 2l - 1, \\ \beta_k &= \frac{1}{\sqrt{N}} \sum_l e^{-ikl} c_j, & j = 2l. \end{aligned} \quad (5)$$

This transformation block diagonalizes the Hamiltonian with translational symmetry, that is,

$$H_0 = \sum_k H_k = \sum_k \psi_k^\dagger h_k \psi_k, \quad (6)$$

where

$$\begin{aligned} H_k &= \frac{1}{2} [\gamma_k (\alpha_{-k}^\dagger \beta_{-k} + \beta_{-k} \alpha_k + \alpha_{-k}^\dagger \beta_k^\dagger + \beta_k^\dagger \alpha_k) + \text{H.c.}] \\ &\quad - g (\alpha_{-k} \alpha_{-k}^\dagger - \alpha_k^\dagger \alpha_k - \beta_{-k} \beta_{-k}^\dagger + \beta_k^\dagger \beta_k) \end{aligned} \quad (7)$$

satisfies the relation $[H_k, H_{k'}] = 0$. Here the core matrix h_k obeys

$$h_k = \begin{pmatrix} 0 & 0 & \gamma_{-k} & -g \\ 0 & 0 & -g & 0 \\ \gamma_k & -g & 0 & 0 \\ -g & 0 & 0 & 0 \end{pmatrix}, \quad (8)$$

which is based on the basis vector

$$\psi_k = \frac{1}{\sqrt{2}} \begin{pmatrix} -\alpha_{-k}^\dagger + \alpha_k \\ -\beta_{-k}^\dagger + \beta_k \\ \beta_{-k}^\dagger + \beta_k \\ -\alpha_{-k}^\dagger - \alpha_k \end{pmatrix}, \quad (9)$$

where $\gamma_k = (1 - \delta) + (1 + \delta)e^{ik}$. The eigenvector with an eigenvalue can be solved as

$$\varepsilon_{\rho\sigma}^k = \frac{\rho}{\sqrt{2}} \sqrt{\Lambda_k + \sigma \sqrt{\Lambda_k^2 - 4g^4}} \quad (10)$$

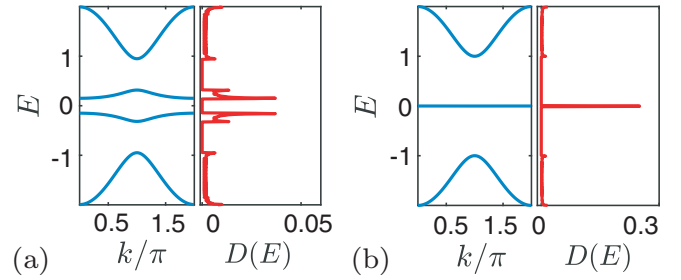


FIG. 2. Plots of the Bogoliubov-de Gennes energy bands for two typical conditions (a) $g = 0.4$ and (b) $g = 0.001$, as a function of momentum k (blue line) and $D(E)$ (red line), respectively. Notably, the flat band energy value and the infinite DOS value both occur when $g \rightarrow 0$. The size of the system is $N = 250$, and the parameters are $\Delta = 0$ and $\delta = 0.2$.

and

$$|\phi_{\rho\sigma}^k\rangle = \frac{1}{\Omega_{\rho\sigma}} \begin{pmatrix} \varepsilon_{\rho\sigma}^k g \gamma_{-k} \\ \varepsilon_{\rho\sigma}^k [(\varepsilon_{\rho\sigma}^k)^2 - g^2] \\ g [(\varepsilon_{\rho\sigma}^k)^2 - g^2] \\ -g^2 \gamma_{-k} \end{pmatrix}, \quad (11)$$

where the parameters satisfy $\sigma, \rho = \pm$ and $\Lambda_k = |\gamma_k|^2 + 2g^2$. The normalization factors are $\Omega_{\rho\sigma} = \rho \sqrt{2g(\varepsilon_{\rho\sigma}^k)^{-1} \{[(\varepsilon_{\rho\sigma}^k)^4 - g^4][(\varepsilon_{\rho\sigma}^k)^2 - g^2]\}^{1/2}}$. There are four Bogoliubov-de Gennes bands from the eigenvalues of h_k , indexed by $\rho, \sigma = \pm$. In this study we considered the case with the band-touching points for ε_{+-}^k and ε_{-+}^k , which occur at k_c . The solution of

$$\Lambda_{k_c} = \sqrt{\Lambda_{k_c}^2 - 4g^4} \quad (12)$$

obeys

$$g = 0, k_c \in (0, 2\pi], \quad (13)$$

which induces the flat zero band. These flat bands can result in an N -order degree of degeneracy, which is a crucial motivation for this work. We plot the energy structures and DOS for two typical conditions, namely $g = 0.4$ and $g = 0.001$, in Fig. 2.

Unlike the twisted graphene, the purpose of creating a moiré pattern here was not to induce a spin-liquid-like phase (the flat Majorana band) but to transition to a new phase in some regions. The flat Majorana band is the inherent property of the spin-liquid-like phase ($g = 0$) in this model. Our motivations for studying this model can be summarized as follows. (i) We aimed to provide an example of the quantum spin systems which can exhibit a moiré pattern, and demonstrate that alternate quantum phases can be found in this one-dimensional dimerized Kitaev spin model with the modulated sinusoidal magnetic field. (ii) As an application, precise control of the quantum phase can be realized in this model, that is, a slight change of Δ can result in distinct quantum phases.

III. MAGNETIZATION, DOS, AND STRING CORRELATION FUNCTION

For the uniform system ($\Delta = 0$) studied here, the ground state is strongly determined by the magnitude g . This viewpoint can be observed from two limits: in strong limit $|g| \gg 1$, the ground state is a Néel magnet with staggered spin alignment. For $g = 0$, the corresponding Hamiltonian has been systematically studied [20]. In medium g , the crossover ground state can be obtained from the exact solution. In this section we utilize three parameters—magnetization, DOS, and string correlation function (SCF)—to characterize the ground-state properties.

(i) The staggered magnetization on site j is defined as

$$m_j^z \equiv (-1)^j \langle G | \sigma_j^z | G \rangle \quad (14)$$

for ground state $|G\rangle$. According to the Hellmann-Feynman theorem, we have

$$m_j^z = (-1)^j \frac{1}{2N} \langle G | \frac{\partial H}{\partial g_j} | G \rangle = (-1)^j \frac{\partial E_g}{\partial g_j}, \quad (15)$$

where E_g is the energy density of the many-body ground state. For the uniform system with zero Δ , m_j^z can be expressed as a function of (δ, g) , that is,

$$m_z = m_j^z = \frac{\partial E_g}{\partial g}. \quad (16)$$

With the exact solution

$$\begin{aligned} E_g &= \frac{1}{4\pi} \int_{-\pi}^{\pi} (\varepsilon_{-+}^k + \varepsilon_{--}^k) dk \\ &= -\frac{2\sqrt{1+g^2}}{\pi} \left[E \left(\frac{1-\delta^2}{1+g^2} \right) \right], \end{aligned} \quad (17)$$

in Sec. II, m_z can be exactly obtained as

$$m_z = -2g \left[E \left(\frac{1-\delta^2}{1+g^2} \right) \right] / (\pi \sqrt{1+g^2}). \quad (18)$$

Here $E(t)$ is the complete elliptic integral. Notably, the parameter satisfies $m_z = 0$ when $g = 0$, which demonstrates one of the characteristics of quantum spin liquid [20]. For clarity, the results of m_z along g for different δ values are plotted in Fig. 3, which indicates that the δ values have a weak effect on m_z .

(ii) The DOS for the Bogoliubov–de Gennes band is defined as

$$D(E) = \lambda \frac{d\mathcal{N}(E)}{dE} \quad (19)$$

generally, $d\mathcal{N}(E)$ indicates the number of energy levels that appear in the interval $[E, E + dE]$, with the normalization factors $\lambda = \Delta E / 4N$. Notably, the result $D(E) \rightarrow \infty$ accords with the fact that flat bands occur at $g = 0$ (Fig. 2).

(iii) The correlation length of the quantum spin model can also demonstrate the characteristics of the spin-liquid phase. Therefore, we introduce the SCF for the ground state, which

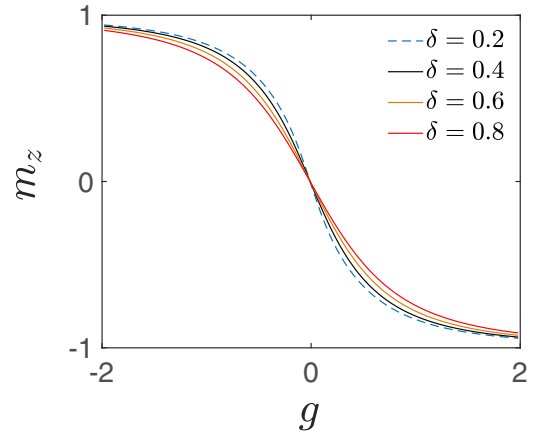


FIG. 3. Plot of the magnetization m_z in Eq. (18) as a function of the on-site potential g for four typical conditions: $\delta = 0.2$ (blue dashed line), $\delta = 0.4$ (black solid line), $\delta = 0.6$ (orange solid line), and $\delta = 0.8$ (red solid line). The computation is performed by using direct diagonalization of Eq. (2). The size of the system is $N = 250$. It indicates that the δ values have a weak effect on m_z .

is defined in

$$\begin{aligned} &O_x^{(2r+1)}[2j-1, 2(j+r)] \\ &= \langle G | \sigma_{2j-1}^x \left(\prod_{n=2j}^{2(j+r)-1} \sigma_n^z \right) \sigma_{2(j+r)}^x | G \rangle. \end{aligned} \quad (20)$$

For estimating the correlation length of the SCF, we consider a perturbed Hamiltonian

$$H^{(2r+1)} = H + c \sum_j \sigma_{2j-1}^x \left(\prod_{n=2j}^{2(j+r)-1} \sigma_n^z \right) \sigma_{2(j+r)}^x, \quad (21)$$

where the extra term stands for the long-range spin-spin coupling with strength c and $H^{(2r+1)}$ is a auxiliary Hamiltonian, the results of the SCF in the following require the condition $c = 0$. The corresponding eigenvalue equation for the ground state is

$$H^{(2r+1)} |G^{(2r+1)}\rangle = E_g^{(2r+1)} |G^{(2r+1)}\rangle, \quad (22)$$

where the energy density of the many-body ground state $E_{g,j}^{(2r+1)}$ can be exactly obtained as

$$\begin{aligned} E_g^{(2r+1)} &= -\frac{1}{4\pi} \int_{-\pi}^{\pi} \{ (1-\delta)^2 + (1+\delta)^2 + c^2 \\ &\quad + 2(1-\delta)(1+\delta) \cos k + 2c(1-\delta) \\ &\quad \times \cos(rk) + 2c(1+\delta) \cos[(r+1)k] \\ &\quad + 4g^2 \}^{(1/2)} dk \end{aligned} \quad (23)$$

by the translational symmetry of $H^{(2r+1)}$. Meanwhile, the translational symmetry of $|G^{(2r+1)}\rangle$ results in

$$\begin{aligned} &O_x^{(2r+1)}[2j-1, 2(j+r)] \\ &= O_x^{(2r+1)}[2(j+l)-1, 2(j+r+l)] \\ &= O_x^{(2r+1)}. \end{aligned} \quad (24)$$

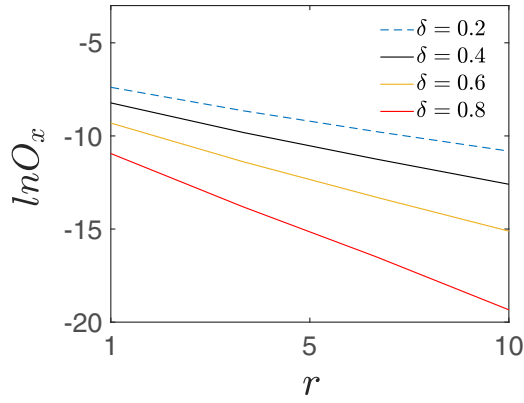


FIG. 4. Plot of the $\ln O_x$ in Eq. (25) on a uniform system for four typical classes of parameters [$\delta = 0.2$ (blue dashed line), $\delta = 0.4$ (black solid line), $\delta = 0.6$ (orange solid line), and $\delta = 0.8$ (red solid line)], as a function of the long-range length r . The computation is performed by using direct diagonalization of Eq. (21). The $\ln O_x$ decreases linearly with r , which satisfies the conclusion in Eq. (26). The size of the system is $N = 250$ and the parameter is $g = 0.4$.

According to the Hellmann-Feynman theorem, the SCF can be expressed as

$$\begin{aligned} O_x^{(2r+1)} &= \left[\frac{\partial E_g^{(2r+1)}}{\partial c} \right]_{c=0} \\ &= - \int_{-\pi}^{\pi} \frac{1}{4\pi\sqrt{2}} \{ (1-\delta)\cos(rk) + (1+\delta) \\ &\quad \times \cos[(r+1)k] \} [(1+\delta^2) + (1-\delta^2) \\ &\quad \times \cos k + 2g^2]^{-1/2} dk, \end{aligned} \quad (25)$$

and $O_x^{(2r+1)}$ satisfies the relation

$$O_x^{(2r+1)} e^{-\frac{2r+1}{\xi}}, \quad (26)$$

which can be transformed into

$$\xi = 2[\ln O_x^{(2r+1)} - \ln O_x^{(2r+3)}]^{-1}. \quad (27)$$

Figure 4 numerically demonstrates the linear relation in Eq. (27). ξ is also determined by g , and $\xi = 0$ occurs at the large limit of g (Fig. 5).

In conclusion, this system has multiple-degenerate ground states with zero magnetization, which characterizes the spin-liquid phase, as claimed in a previous study [20]. However, when $g \rightarrow \infty$, $\xi \rightarrow 0$ and $m_z \rightarrow 1$, which indicates the Néel phase.

IV. MOIRÉ FRINGES

The aim of this work was to present the moiré fringes of the system with nonzero Δ and the properties of the system with zero Δ ; however, different g , as discussed in Sec. III, should appear in the different locations along the system. Considering magnetization m_j^z as a function of the coordinate, we introduce LDOS to replace DOS. For calculating such parameters, the solution of H is necessary. We utilize Majorana fermion operators

$$a_j = c_j^\dagger + c_j, b_j = -i(c_j^\dagger - c_j), \quad (28)$$

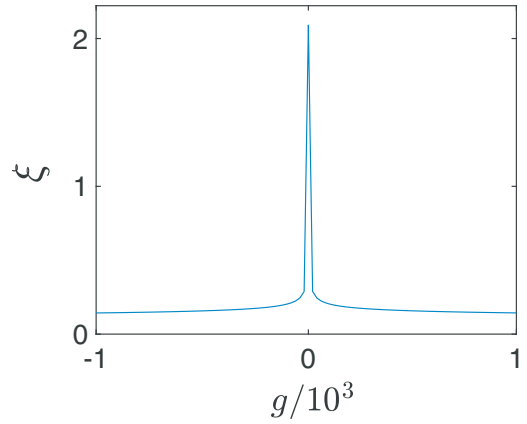


FIG. 5. Plot of the correlation length ξ in Eq. (27) as a function of the on-site potential g . The computation is performed by using direct diagonalization of Eq. (21). The correlation length ξ is finite when $g \rightarrow 0$, whereas ξ decays rapidly to zero as $|g|$ increases. The size of system is $N = 250$, and the parameter is $\delta = 0.2$.

which satisfy the relations

$$\{a_j, a_{j'}\} = 2\delta_{j,j'}, \quad \{b_j, b_{j'}\} = 2\delta_{j,j'}, \quad (29)$$

and

$$\{a_j, b_{j'}\} = 0, \quad a_j^2 = b_j^2 = 1. \quad (30)$$

The inverse transformation obeys

$$c_j^\dagger = \frac{1}{2}(a_j + ib_j), \quad c_j = \frac{1}{2}(a_j - ib_j). \quad (31)$$

Then the Majorana representation of Hamiltonian is

$$H = \psi^T h \psi, \quad (32)$$

where $\psi^T = (ia_1, b_1, ia_2, b_2, ia_3, b_3, \dots, ia_{2N}, b_{2N})$. Here h represents a $4N \times 4N$ matrix, which can be explicitly written as

$$\begin{aligned} h &= \frac{g}{2} \sum_{j=1}^{2N} (-1)^j \cos(j\pi\Delta) |j\rangle_{ab} \langle j| \\ &\quad + \frac{1}{2} \sum_{j=1}^N [(1+\delta)|2j\rangle_{ab} \langle 2j+1| \\ &\quad + (1-\delta)|2j\rangle_{ab} \langle 2j-1|] + \text{H.c.}, \end{aligned} \quad (33)$$

where $|j\rangle_\lambda$ ($\lambda = a, b$) is a single-particle orthonormal complete set, which satisfies ${}_\lambda \langle j|j'\rangle_{\lambda'} = \delta_{\lambda\lambda'} \delta_{jj'}$, $j \in [1, 2N]$, and ${}_b \langle 2N+1| \equiv 0$. Obviously h describes a single-particle tight-binding SSH model with side couplings and cosine-modulated couplings. The schematic of the Majorana lattice system is sketched in Fig. 6.

Then ground-state energy E_g , m_j^z , and D_j (LDOS) can also be obtained by diagonalizing the matrix of the lattice system. For the ground state, the Majorana operators a_{2j-1} and b_{2j} are free in the $g_j = 0$ region, resulting in numerous degenerate ground states. We depict the magnetization as a function of j [Fig. 7(a)] and compute D_j by using the method [23] [Fig. 7(b)]. Inspired by the characteristics of the SCF, we consider an artificial model with non-neighbour interactions,

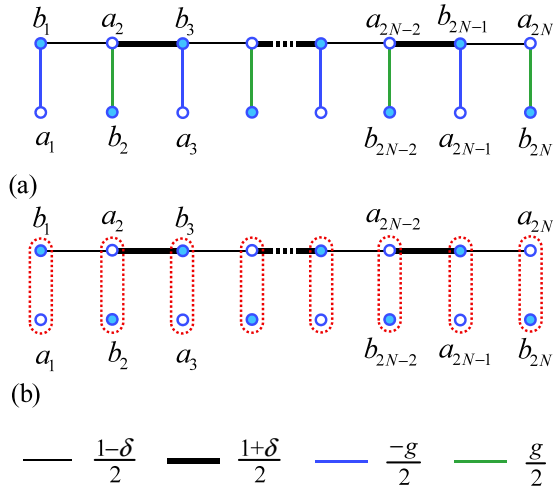


FIG. 6. Lattice geometries for the Majorana models, which are described in Eq. (33). The solid (empty) circle indicates (anti) Majorana modes. (a) The SSH model with side-couplings $(1 \pm \delta)/2$ and $\pm g/2$. In (b), $g = 0$.

and the Hamiltonian obeys

$$h_j^{(2r+1)} = h + \frac{c}{2} (|2j + 2r\rangle_{ab} \langle 2j - 1| + \text{H.c.}), \quad (34)$$

which is the mapping of the Hamiltonian in Eq. (21). The energy density of the ground state $E_{g,j}^{(2r+1)}$ for the many-body system equals the sum of all negative eigenvalues from $h_j^{(2r+1)}$ with the coefficient $1/(2N)$, which can be numerically obtained. The corresponding SCF and ξ can be computed from the relation

$$O_{x,j}^{(2r+1)} = \lim_{c \rightarrow 0} \frac{\partial E_{g,j}^{(2r+1)}}{\partial c}, \quad (35)$$

and we have the equation

$$\xi_j = 2[\ln O_{x,j}^{(2r+1)} - \ln O_{x,j}^{(2r+3)}]^{-1}. \quad (36)$$

We depict ξ_j as a function of j in Fig. 7(c), which demonstrates the above analyses of the moiré fringes system.

V. DYNAMIC DETECTION

The investigation in this section may provide the scheme to experimentally detect the moiré fringes. Realizing a quantum spin system with the Hamiltonian H is a challenge because the moiré pattern appears in a relatively large system. In this sense, both spin and Kitaev p -wave system is hard to implement. However, as shown above, a moiré pattern is also reflected in the quasiparticle spectrum of the spin model, that is, the LDOS, or the spectral structure of the corresponding Majorana dual of the spin system. The Majorana lattice in Eq. (33) is essentially an extended version of the SSH model. Recently, many works on the experimental realization of the SSH model in the photonic system have been reported.

The Majorana lattice h appears as a relatively simpler structure, which can be arranged in a photonic system [14,15]. It is based on the analogy between light propagating through a photonic crystal and a tight-binding Hamiltonian. For example, topological effects in some electronic systems can be

observed in their photonic counterpart [24–28]. In a photonic platform, Pauli exclusion is not obeyed, a single-particle state can be amplified by the large population of photons. It allows for a high degree of control over the system parameters.

In this section we consider the Hamiltonian h_η with a slight perturbation for investigating the dynamical signature of the moiré pattern, the Hamiltonian h_η does not break the symmetry of the original Hamiltonian [29] and has the form

$$h_\eta = h + \eta \sum_{j=1}^{2N} (|j\rangle_{ba} \langle j| + \text{H.c.}), \quad (37)$$

where the perturbation is a transverse field with the strength η . We employ the LE to investigate the dynamical signature of the moiré pattern. The LE for an initial state $|\psi_0\rangle$ is defined as

$$M(t) = |\langle \psi_0 | \exp(ih_\eta t) \exp(-iht) | \psi_0 \rangle|^2. \quad (38)$$

We take $|\psi_0\rangle$ as the initial state, which is the site state at the j th site; thus, $M(t)$ is a function of position j , which is labeled by $M_j(t)$. Numerical simulations demonstrate that the LE decays in the form

$$M_j(t) = e^{-\gamma_j t^2}; \quad (39)$$

thus we have

$$\Gamma_j(t) = \sqrt{-\ln M_j(t)} = \sqrt{\gamma_j} t. \quad (40)$$

The parameter $\Gamma_j(t)$ is introduced to present the decay behaviour, as a function of evolution time t (Fig. 8). Furthermore, we depict the decay of LE (γ_j) as a function of site j [Fig. 7(d)]. For clarity, we demonstrate the relations of calculated LE for a series of j and t values (Fig. 9). Notably, the performances of Γ , γ , and M , which are described in the three aforementioned figures, cannot be affected by the varied parameters δ . Such a moiré pattern can be implemented through weakly coupled waveguide arrays.

In the following we present a scheme of experimentally detection of LE for the Majorana lattices in Eqs. (33) and (37) via a system of waveguide arrays. We consider a quasi-one-dimensional array made of $4N$ equal straight waveguides, which are assumed to be weakly coupled. The geometry of the system is schematically illustrated in Fig. 10, which consists of four sections along the direction of light propagation z . According to the coupled-mode theory, the light propagation can be described by Schrödinger-like equation, which is usually to be used to mimic the dynamics of a tight-binding system.

For the first and third sections with length $L/2$, the corresponding equations are

$$i \frac{\partial u(z)}{\partial z} = hu(z), \quad (41)$$

for $z \in [0, L/2]$ and

$$i \frac{\partial u(z)}{\partial z} = h_\eta u(z), \quad (42)$$

for $z \in (L/2, L]$, respectively. Here the vector has the form $u(z) = [u_{a,1}(z), u_{b,1}(z), \dots, u_{a,2N}(z), u_{b,2N}(z)]^T$, with the component $u_{\lambda,l}(z)$ denotes the mode amplitude in the corresponding waveguide, where $\lambda = a, b$ and $l = 1, 2, \dots, 2N$.

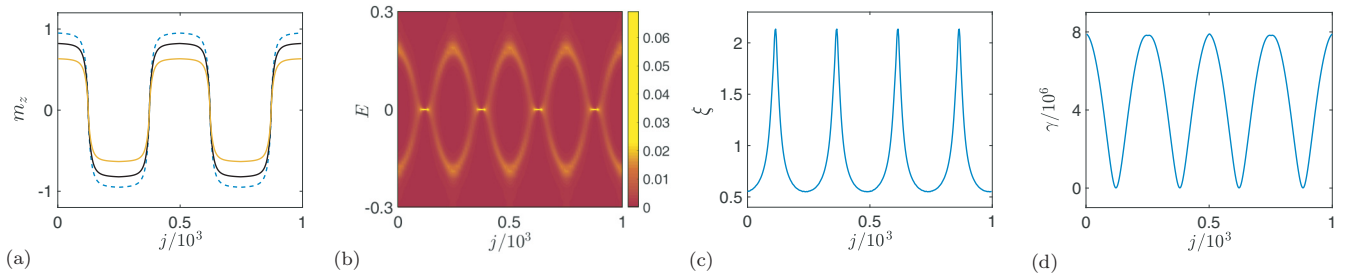


FIG. 7. Numerical simulations of four typical parameters, [(a) magnetization (m_z), (b) local density of state (LDOS), (c) correlation length (ξ), and (d) decay of the LE (γ)] as a function of site j . Computations are all performed by using a uniform mesh in the position j discretization for typical parameters. These panels are the main results of the present study. (a) On-site potential amplitude parameters are $g = -2.5$ (blue dashed line), $g = -1$ (black solid line), and $g = -0.5$ (orange solid line). The top (or valley) of the magnetization depends on the value of g in (a). All panels exhibit unitary moiré patterns for a infinite site system. Parameter in (d) is $\eta = 0.005$. The size of system is $N = 250$, and the common parameters are $\Delta = 0.004$, $g = 0.4$, and $\delta = 0.2$.

The second and fourth sections are the waveguides with segmentation at $z = L/2$ and L , supporting the function of sudden change π phase on the mode amplitudes of one of two sublattices [16,17]. Explicitly, the action of such two sections is a transformation

$$U = \begin{pmatrix} 1 & 0 & 0 & 0 & 0 \\ 0 & -1 & 0 & 0 & 0 \\ 0 & 0 & \ddots & 0 & 0 \\ 0 & 0 & 0 & 1 & 0 \\ 0 & 0 & 0 & 0 & -1 \end{pmatrix}. \quad (43)$$

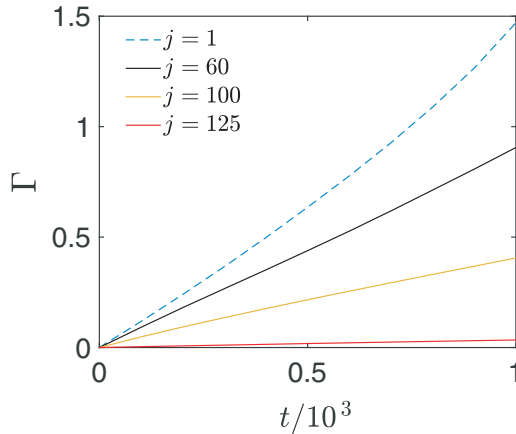


FIG. 8. Numerical simulations of the decay behavior (Γ) of Loschmidt echo (LE) [Eq. (40)] on a slight perturbation Hamiltonian for four typical site classes $j = 1$ (blue dashed line), $j = 60$ (black solid line), $j = 100$ (orange solid line), and $j = 125$ (red solid line) as a function of time evolution t . The computation is performed by using a uniform mesh in the time discretization for the time-dependent $\Gamma(t)$. We take the site state at the j th site. The $\Gamma(t)$ increases linearly and approximately with time t , which is associated with the correlation showed in Eq. (39). When the periodicity of the moiré pattern is considered, the results of $\Gamma(t)$ along the site j from 1 to 125 (1/4 period) illustrate the properties of the integral period. The system parameters are $N = 250$, $\Delta = 0.004$, $\eta = 0.005$, $g = 0.4$, and $\delta = 0.2$.

Accordingly, for a given initial wave function $u(0)$, we have

$$\begin{aligned} u(L^-/2) &= e^{-ihL/2}u(0), \\ u(L^+/2) &= Uu(L^-/2), \\ u(L^-) &= e^{-ih_\eta L/2}u(L^+/2), \\ u(L^+) &= Uu(L^-), \end{aligned} \quad (44)$$

where $L^\pm = L + 0^\pm$. We note that

$$Ue^{-ih_\eta z}U^{-1} = e^{-i(-h_\eta)z} = e^{-ih_\eta(-z)}, \quad (45)$$

due to the fact

$$UQU^{-1} = -Q \quad (46)$$

for an arbitrary Hamiltonian matrix Q describing a single-particle tight-binding bipartite lattice without on-site potential. Obviously the action of the sandwich (second-third-fourth section) is equivalent to the time-reversal evolution operator for h_η . According to Eq. (38), the LE at L can be

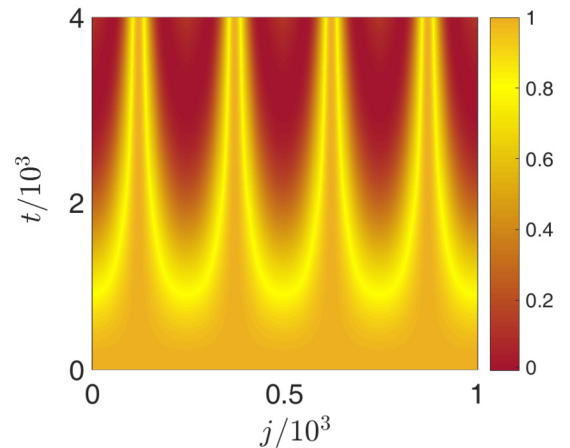


FIG. 9. Numerical simulation of LE in Eq. (38) as a function of site-state j and evolution time t in the Majorana model. The computation is performed by using uniform meshes in the time and position discretization for the LE. The periodic behavior is obvious, exhibiting a moiré pattern as expected. We take the site state at the j th site. The size of system is $N = 250$, and the parameters are $\Delta = 0.004$, $\delta = 0.2$, $g = 0.4$, and $\eta = 0.005$.

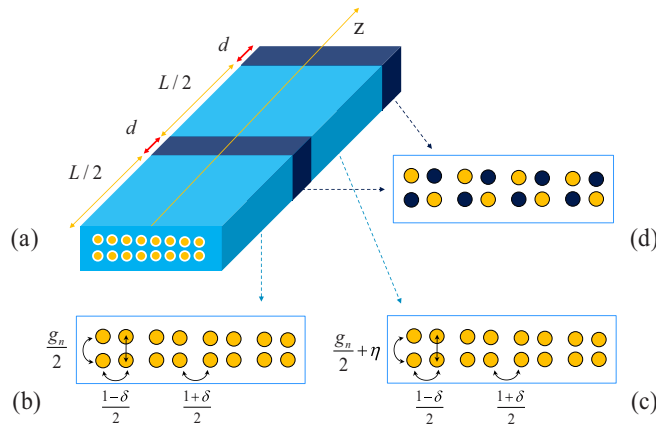


FIG. 10. Sketch of the quasi-one-dimensional waveguide array to mimic the Majorana lattices in Eqs. (33) and (37). (a) There are four array sections. (b) and (c) Waveguide array sections for h and h_η , respectively. The length is $L/2$, and the strength of the evanescent couplings are indicated. (d) Waveguide array sections for U , with segmentation at sublattice denoted by dark blue circles. The length is d , much smaller than L .

measured experimentally by

$$\begin{aligned}
 M(L^+) &= |u^*(0)e^{ih_\eta L/2}e^{-ihL/2}u(0)|^2 \\
 &= |u^*(0)Ue^{-ih_\eta L/2}U^{-1}e^{-ihL/2}u(0)|^2 \\
 &= |u^*(0)u(L^+)|^2 \\
 &= \sum_{m=a}^b \sum_{n=1}^{2n} |u_{m,n}^*(0)u_{m,n}(L^+)|^2. \quad (47)
 \end{aligned}$$

If we take a series of site states as initial states, i.e., $u(0) = u_{m_0, n_0}(0) = u_j(0) = 1$ and take light propagation distance z as time t , then apply Eq. (47), we have

$$\begin{aligned}
 M_j(L^+) &= |u_j^*(0)u_j(L^+)|^2 \\
 &= |u_j(L^+)|^2, \quad (48)
 \end{aligned}$$

which correspond to the numerical results of Fig. 9.

This demonstrates that detecting the moiré fringes via LE is possible in arrays of coupled waveguides in the aid of segmented sections. This scheme is independent of the geometry of the array and therefore provides a way to measure the LE in a tight-binding model.

VI. SUMMARY

In summary, we have demonstrated that a superperiodicity in the coordinate space along a quantum spin system is imposed on it if the beat period of the external sinusoidal magnetic field has a slight difference with the lattice constants. There are two quantum phases in each period, one is Néel phase, another is spin liquid phase. As a huge unit cell, the phase diagram is presented and repeated when the coordinate changes in real space, rather than varying the external field. The moiré system provides a new way to study the phenomena related to quantum phases. An advantage of this scheme is that one needs not to control the field dynamically. The process to vary a parameter is challenging in practice. However, one can simulate the crossover by simply setting a slightly different but commensurate periods of two ingredients of the system. Additionally, we have proposed a dynamic scheme to detect the moiré fringes based on the measurement of LE with the respect to local perturbation. We employed arrays of coupled waveguides to stimulate the dynamic process in the Majorana lattice. It has been demonstrated that detecting the moiré fringes via LE is possible in the aid of segmented sections. This scheme is independent of the geometry of the array. It provides a method to detect the moiré fringes in a photonic system, which is different from the real quantum condensed-matter system, but can reproduce almost all condensed-matter experiments.

ACKNOWLEDGMENT

This work was supported by National Natural Science Foundation of China (under Grant No. 11874225).

-
- [1] M. Yankowitz, J. Xue, D. Cormode, J. D. Sanchez-Yamagishi, K. Watanabe, T. Taniguchi, P. Jarillo-Herrero, P. Jacquod, and B. J. LeRoy, Emergence of superlattice Dirac points in graphene on hexagonal boron nitride, *Nat. Phys.* **8**, 382 (2012).
- [2] L. A. Ponomarenko, R. V. Gorbachev, G. L. Yu, D. C. Elias, R. Jalil, A. A. Patel, A. Mishchenko, A. S. Mayorov, C. R. Woods, J. R. Wallbank, M. Mucha-Kruczynski, B. A. Piot, M. Potemski, I. V. Grigorieva, K. S. Novoselov, F. Guinea, V. I. Fal'ko, and A. K. Geim, Cloning of Dirac fermions in graphene superlattices, *Nature (London)* **497**, 594 (2013).
- [3] C. R. Dean, L. Wang, P. Maher, C. Forsythe, F. Ghahari, Y. Gao, J. Katoch, M. Ishigami, P. Moon, M. Koshino, T. Taniguchi, K. Watanabe, K. L. Shepard, J. Hone, and P. Kim, Hofstadter's butterfly and the fractal quantum Hall effect in moiré superlattices, *Nature (London)* **497**, 598 (2013).
- [4] B. Hunt, J. Sanchez-Yamagishi, A. Young, M. Yankowitz, B. J. LeRoy, K. Watanabe, T. Taniguchi, P. Moon, M. Koshino, P. Jarillo-Herrero, and R. C. Ashoori, Massive Dirac fermions and Hofstadter butterfly in a van der Waals heterostructure, *Science* **340**, 1427 (2013).
- [5] C. R. Woods, L. Britnell, A. Eckmann, R. S. Ma, J. C. Lu, H. M. Guo, X. Lin, G. L. Yu, Y. Cao, R. V. Gorbachev, A. V. Kretinin, J. Park, L. A. Ponomarenko, M. I. Katsnelson, Yu. N. Gornostyrev, K. Watanabe, T. Taniguchi, C. Casiraghi, H-J. Gao, A. K. Geim, and K. S. Novoselov, Commensurate-incommensurate transition in graphene on hexagonal boron nitride, *Nat. Phys.* **10**, 451 (2014).
- [6] S. Nakajima, T. Tomita, S. Taie, T. Ichinose, H. Ozawa, L. Wang, M. Troyer, and Y. Takahashi, Topological Thouless pumping of ultracold fermions, *Nat. Phys.* **12**, 296 (2016).
- [7] M. Lohse, C. Schweizer, O. Zilberberg, M. Aidelsburger, and I. Bloch, A Thouless quantum pump with ultracold bosonic atoms in an optical superlattice, *Nat. Phys.* **12**, 350 (2016).

- [8] R. V. Gorbachev, J. C. W. Song, G. L. Yu, A. V. Kretinin, F. Withers, Y. Cao, A. Mishchenko, I. V. Grigorieva, K. S. Novoselov, L. S. Levitov, and A. K. Geim, Detecting topological currents in graphene superlattices, *Science* **346**, 448 (2014).
- [9] J. C. W. Song, P. Samutpraphoot, and L. S. Levitov, Topological Bloch bands in graphene superlattices, *Proc. Natl. Acad. Sci. U.S.A.* **112**, 10879 (2015).
- [10] J. Jung, A. Raoux, Z. Qiao, and A. H. MacDonald, *Ab initio* theory of moiré superlattice bands in layered two-dimensional materials, *Phys. Rev. B* **89**, 205414 (2014).
- [11] X. M. Yang, X. Z. Zhang, C. Li, and Z. Song, Dynamical signature of the moiré pattern in a non-Hermitian ladder, *Phys. Rev. B* **98**, 085306 (2018).
- [12] H. A. Haus and W. Huang, Coupled-mode theory, *Proc. IEEE* **79**, 1505 (1991).
- [13] A. Szameit and S. Nolte, Discrete optics in femtosecond-laserwritten photonic structures, *J. Phys. B: At. Mol. Opt. Phys.* **43**, 163001 (2010).
- [14] L. Lu, J. D. Joannopoulos, and M. Soljačić, Topological photonics, *Nat. Photon.* **8**, 821 (2014).
- [15] T. Ozawa, H. M. Price, A. Amo, N. Goldman, M. Hafezi, L. Lu, M. C. Rechtsman, D. Schuster, J. Simon, O. Zilberberg, and I. Carusotto, Topological photonics, *Rev. Mod. Phys.* **91**, 015006 (2019).
- [16] S. Longhi, Image reconstruction in segmented waveguide arrays, *Opt. Lett.* **33**, 473 (2008).
- [17] A. Szameit, F. Dreisow, M. Heinrich, T. Pertsch, S. Nolte, A. Tünnermann, E. Suran, F. Louradour, A. Barthélémy, and S. Longhi, Image reconstruction in segmented femtosecond laser-written waveguide arrays, *Appl. Phys. Lett.* **93**, 181109 (2008).
- [18] A. Kitaev, Anyons in an exactly solved model and beyond, *Ann. Phys.* **321**, 2 (2016).
- [19] X.-Y. Feng, G.-M. Zhang, and T. Xiang, Topological Characterization of Quantum Phase Transitions in a Spin-1/2 Model, *Phys. Rev. Lett.* **98**, 087204 (2007).
- [20] K. Le Hur, A. Soret, and F. Yang, Majorana spin liquids, topology, and superconductivity in ladders, *Phys. Rev. B* **96**, 205109 (2017).
- [21] R. Wang, C. Li, X. Z. Zhang, and Z. Song, Dynamical bulk-edge correspondence for degeneracy lines in parameter space, *Phys. Rev. B* **98**, 014303 (2018).
- [22] P. Jordan and E. Wigner, About the Pauli exclusion principle, *Z. Phys.* **47**, 631 (1928).
- [23] R. Haydock, The recursive solution of the Schrödinger equation, *Comput. Phys. Commun.* **20**, 11 (1980).
- [24] M. C. Rechtsman, Y. Plotnik, J. M. Zeuner, D. Song, Z. Chen, A. Szameit, and M. Segev, Topological Creation and Destruction of Edge States in Photonic Graphene, *Phys. Rev. Lett.* **111**, 103901 (2013).
- [25] Y. Plotnik, M. C. Rechtsman, D. Song, M. Heinrich, J. M. Zeuner, S. Nolte, Y. Lumer, N. Malkova, J. Xu, A. Szameit, Z. Chen, and M. Segev, Observation of unconventional edge states in ‘photonic graphene’, *Nat. Mater.* **13**, 57 (2014).
- [26] S. Stützer, Y. Plotnik, Y. Lumer, P. Titum, N. H. Lindner, M. Segev, M. C. Rechtsman, and A. Szameit, Photonic topological Anderson insulators, *Nature (London)* **560**, 461 (2018).
- [27] J. Noh, W. A. Benalcazar, S. Huang, M. J. Collins, K. P. Chen, T. L. Hughes, and M. C. Rechtsman, Topological protection of photonic mid-gap defect modes, *Nat. Photon.* **12**, 408 (2018).
- [28] M. Hafezi, S. Mittal, J. Fan, A. Migdall, and J. M. Taylor, Imaging topological edge states in silicon photonics, *Nat. Photon.* **7**, 1001 (2013).
- [29] The original Hamiltonian has the rotation symmetry $[R, H] = 0$, where the operator $R = \prod_{j=1}^{2N} \exp[i\pi\sigma_j^z/2]$ with the action $R\sigma_j^z R^{-1} = \sigma_j^z$, $R\sigma_j^x R^{-1} = -\sigma_j^x$, and $R\sigma_j^y R^{-1} = -\sigma_j^y$. Such symmetry rules out the longitudinal field. Then the slight perturbed model in original Eq. (37) does not break the symmetry.